Renewable Energy 168 (2021) 64–75

Contents lists available at ScienceDirect

Renewable Energy

journal homepage: www.elsevier.com/locate/renene

The performance of a weir-mounted tidal turbine: An experimental investigation

M.C. Verbeek *, R.J. Labeur , W.S.J. Uijttewaal

Faculty of Civil Engineering and Geosciences, Delft University of Technology, the Netherlands

ARTICLE INFO

Article history:
Received 21 July 2020
Received in revised form
24 October 2020
Accepted 4 December 2020
Available online 8 December 2020

Keywords:
Tidal stream turbine
Power output optimisation
Hydraulic structure
Experimental investigation
Wake

ABSTRACT

The tidal flow between bridge pillars and through open barriers is a promising source of ocean energy which can be exploited using tidal stream turbines, as proven recently by operational demonstration plants. The aim of this study is to clarify the consequences for the power output of tidal turbines when placing them in a hydraulic structure. To this end, experimental measurements of turbine power and wakes are performed, using a down-scaled turbine mounted at a submerged weir. The results are compared to an analytical model, validating its range of application for optimising turbine-weir geometries. The experimental data show that the power coefficient of the turbine can be increased by optimising the blockage of the channel and the distance between the turbine and the structure, which is related to the wake configuration. In this way, the power coefficient increased by 40% when the turbine was re-positioned from the upstream to the downstream end of the structure. The theoretical model could reproduce the measured power within 10% accuracy, proving its value as a rapid assessment tool. As such, this work advances the knowledge needed to meet targets on the transition towards renewable energy.

1. Introduction

The EU has targeted to increase the share of renewable energy in the electricity sector from 21% in 2014 to at least 45% in 2030 [1]. Ocean energy can provide a substantial and reliable contribution to the required energy mix [2]. The tidal flow between bridge pillars and through open barriers is a yet unharvested and promising source of ocean energy, which can be exploited using tidal stream turbines. This technology was demonstrated in a Dutch storm surge barrier, where five 250 kW turbines were installed in a gate opening [3,4]. This type of existing barrier is a suitable location for tidal energy harvesting, provided that attention is paid to the structural stability of the barrier and the increased resistance by the turbines. However, it is yet unclear how the power output from these turbines should be maximised when they are mounted inside hydraulic structures.

The underlying problem is that the interaction of a turbine with the flow through hydraulic structures is poorly understood. Many researchers investigated either the hydrodynamics of horizontal-axis turbines (e.g. Ref. [5,6]) or the flow through a hydraulic structure [7], but until now their combination has not been explored. Even-though, three geometry parameters can be listed that mainly influence the structure - turbine interaction. Firstly [3], indicated that the streamwise position of a turbine relative to a weir determines the shape of the turbine wake and hence the power output. Secondly, the ratio between the rotor swept area and the local cross section of the channel, the so-called blockage, affects the energy flux that can be harvested by a turbine in a constrained flow [5]. Lastly [8], showed, using a CFD study of a turbine at a submarine hill, that a streamwise decrease of the water depth at the turbine location is essential to increase the turbine thrust. A systematic analysis of these parameters could unravel optimal design choices, however, the data required for such investigations are missing.

Theoretical models, such as postulated by Ref. [5,9,10]; provide a useful framework to define the type of data that are needed for this purpose. These methods are based on 1D balances of mass, energy, and momentum of the flow passing a turbine that is schematised as an actuator disk [11,12]. Recently, this approach was extended to include a turbine in a hydraulic structure, where the latter is schematised as a step in the bed [3]. From this model, we infer principal indicators of turbine performance that should be measured: e.g., the power coefficient of the turbine, the

* Corresponding author.
E-mail address: m.c.verbeek@tudelft.nl (M.C. Verbeek).

https://doi.org/10.1016/j.renene.2020.12.013

distribution of the flow in the wake and bypass, and the associated pressure recovery in the wake. Besides, these measurements can be compared with the corresponding model predictions, thus verifying the application of these models to complex geometries. This may allow a selection of the associated design parameters using theoretical models which, unlike advanced computational fluid dynamics (CFD), can evaluate the turbine performance for a wide range of input variables using limited computational resources only.

The aim of this research is to clarify the consequences of placing a tidal turbine in a hydraulic structure, using experimental observations. To meet this aim, an experimental turbine with a 1-in-8.6 scale is tested in a flume, in combination with different weir geometries, for which the observed performance characteristics have been related to the observed wake properties. To this end, the influence of three geometrical parameters on the power coefficient and hydrodynamics are evaluated: the weir height, the local blockage, and the streamwise distance between turbine and weir. The results from the model of [3] are compared with the measurements in order to validate the range of application of the model for optimising design parameters in more complex turbine-structure geometries. In this way, this study facilitates an optimal placing and operation of tidal stream turbines in hydraulic structures in order to harvest more power from the ocean, which contributes to the knowledge needed to meet targets on renewable energy production.

This paper has the following structure. First, it is discussed how the experiments are set-up to obtain specific information concerning the turbine power and wake configuration. Subsequently, the experimental data are presented and differences in power output for the different turbine-weir combinations are discussed, in particular how this relates to the wake configuration. Thereafter, the obtained experimental results are compared to the theoretical prediction of the model of [3]. The range of application of this type of theoretical models is discussed and possibilities for optimising the geometry to harvest more power from the flow are explored. The discussion section addresses the implications of mounting a turbine in a barrier, considering the increased resistance of the structure. Finally, conclusions are drawn regarding the power output consequences of placing a turbine in a hydraulic structure.

2. Methods

The experimental set-up is inspired by the hydrodynamics of a weir-mounted turbine in the Eastern Scheldt barrier, The Netherlands, as described by Ref. [3] (Fig. 1a). However, the aim of the experiments is to gain insight in the most important processes rather than accurately reproducing the flow at the test site in the Eastern Scheldt barrier.

To this end the experiments provide information about turbine power and wake configuration when placing a turbine in different hydraulic structure geometries in order to improve our understanding of the relevant physics and to facilitate comparison with theoretical models. The required tests are done with a down-scaled turbine in an experimental flume. The design of the experimental set-up, the data processing, and scaling analysis are explained in this section.

2.1. Experimental set up

A 1-in-8.6 geometrically-scaled T1 turbine from the company Tocardo Power Turbines BV is used (Fig. 2b). The design of the T1 is similar to the prototype T2, which is deployed in the Eastern Scheldt barrier and has a rotor diameter of 5.3 m, except for the relatively thicker hub. The rotor diameter of the T1 equals 3.4 m at full scale and 0.4 m at model scale. The electrical system and mount of the model turbine are especially manufactured for the tests; the blades and hub are provided by Tocardo. The torque is applied by an AC Servo motor and drive, while controlling the turbine at a constant tip speed.

The turbine is mounted in a horizontal, recirculating flume with a length of 40 m, a width of 0.78 m, and a height of 0.85 m in the Laboratory of Environmental Fluid Mechanics of Delft University of Technology, The Netherlands (Fig. 2a). The investigated hydraulic structure concerns a long-crested weir which can be installed at the bed of the flume (details will be given in Sec. 2.3). The discharge in the flume amounted to 0.4 $m^3\ s^{-1}$, and the water level in the flume was 0.65 m or 0.70 m relative to the bed level, depending on the experimental case. This corresponds to an undisturbed flow velocity in the flume of 0.73–0.79 m s^{-1}. The inflow section of the flume features a honeycomb structure, consisting of horizontal parallel pipes to straighten the inflow. All tests are performed for a single streamwise turbulence intensity at the inflow of around 5–7%, which is consistent with a typical offshore site value at hub height [13] and in line with earlier scale tests of e.g. Ref. [6,14].

Three series of tests are conducted in which three geometrical parameters are systematically varied: blockage by the turbine, height of the weir, and streamwise distance between the weir and the turbine, which are defined in Sec. 2.3.3. In particular, attention is payed to the weir-turbine distance as this had a major influence on wake configuration and turbine performance and was not investigated before [3]. Consequently, the turbine is placed at five distances from the weir within each test series. Additionally, two weir heights and two blockages are considered. One reference test without turbine is conducted for each series. The resulting test cases are summarized in Table 1 and one configuration is illustrated as an example in Fig. 1.

Flow data are obtained at vertical transects in the centre line of the flume, for a range of streamwise distances, including - but not limited to - the transects defined in the theoretical model of [3]. Consequently, the profiles at the following streamwise locations are (at least) sampled in each test: the inflow section of the flume, the crest of the hydraulic structure, and the turbine wake at, respectively, three and ten rotor diameters downstream of the turbine, where at the latter location the wake has almost fully recovered [6]. In between these locations, additional velocity transects are obtained at streamwise intervals of one rotor diameter to gain detailed insight on the configuration of the wake (Fig. 1d). Lateral transects at axis height are measured at the inflow section and in the wake at three and ten rotor diameters downstream of the blades for each test. Fig. 1e indicates the locations of these measurements.

2.2. Data processing

Flow velocities are measured with Nortek Vectrino side-looking and down-looking transducers [15]. The device sampling frequency was 25 Hz at an acoustic frequency of 10 MHz. The cylindrical sampling volume had a width and height of 6 mm, and each location was sampled for 3-min intervals. A central data-acquisition system recorded water levels, turbine thrust, turbine torque, turbine tip speed and the flume discharge at 200 Hz during the tests for 3-min up to 15-min intervals. Three minutes is sufficiently long to obtain stationary mean values of flow velocity, turbulence intensity, and turbine load. This is verified with an auto-correlation analysis of the time series and converge check with available longer time series. Water levels are measured with six conductivity meters along the flume centre line. Turbine thrust [N] is measured with a bending beam load cell (version: LSH-100KG, precision class: C3) connected to the turbine strut (Fig. 1b). The turbine torque Q

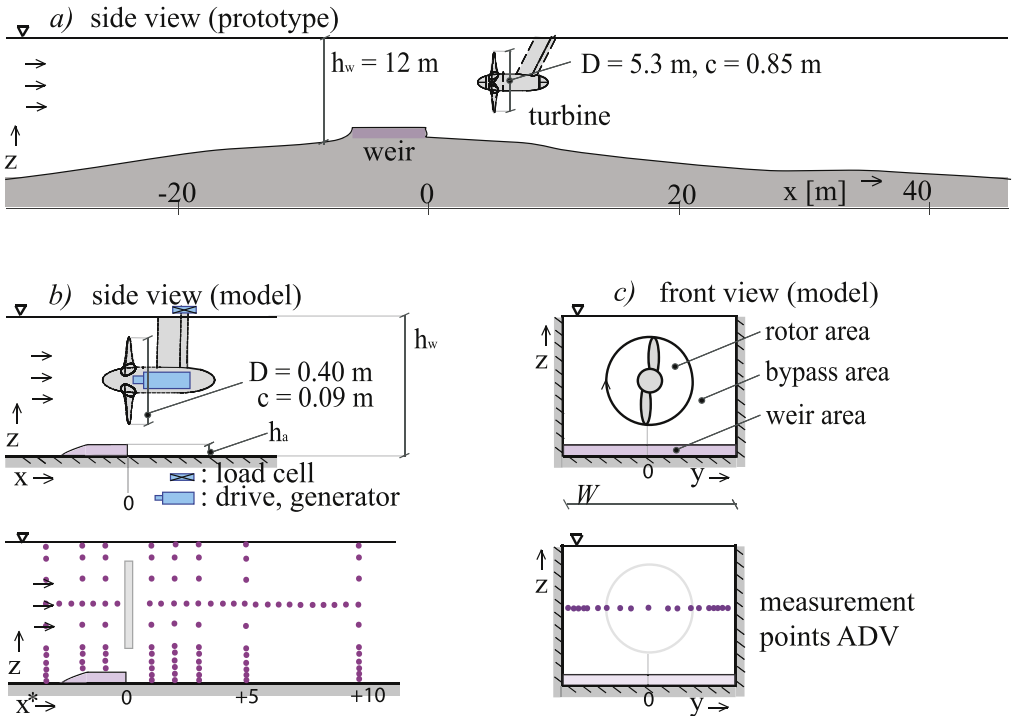

Fig. 1. A schematic drawing of a) the prototype turbine in the Eastern Scheldt, b) the laboratory set-up of a turbine downstream of a broad crested weir in a side view c) and in a front view; the dimensions of the set-up are indicated in the figure; for panel a) and b): D is the rotor diameter, c is the blade chord, h_a is the height of the weir, and h_w is the water depth in the flume; for panel c): W is the flume width; the lower panels show the measurement locations of the velocimeters in side and top view, respectively. Lateral transects are taken at $x^* = -2, 3$, and 10 for each test. Vertical profiles are taken at the flume centreline.

Fig. 2. Photos from the experimental set up: a) the recirculating current flume in the Laboratory of Environmental Fluid Mechanics of Delft University of Technology, The Netherlands, b) the turbine and weir; the turbine is positioned two rotor diameters upstream of the weir end in the picture ($x/D = -2$).

Table 1
Overview of dimensions and scaling parameters of the three series of tests and corresponding values of the prototype of the Eastern Scheldt, The Netherlands; D is the rotor diameter, h_a is the weir height, h_w is the (flume or field) water depth; the definitions of the parameters, B^*, a^*, and x^* are given in Eqs. (8)–(10) and the dynamical parameters Fr, Re, Re_c, and λ are defined in Eqs. (2)–(5), respectively; tests are conducted at a discharge of 0.4 m^3s^{-1}

Parameter	Symbol	Unit	Series 1	Series 2	Series 3	Prototype
Geometry	D	[m]	0.40	0.40	0.40	5.3
	h_a	[m]	0.05	0.10	0.10	3.0
	h_w	[m]	0.65	0.65	0.70	12
	a^*	–	0.08	0.15	0.14	0.25
	B^*	–	0.25	0.25	0.23	0.24
	x^*	–	$-2, -1, 0, 1, 2$	$-2, 0, 1$	$-2, 0, 1$	1
Dynamics	λ	–	[0, 10]	4	4	4
	Fr	–	0.36	0.36	0.31	0.28
	Re	–	$5.0 \cdot 10^5$	$5.0 \cdot 10^5$	$5.0 \cdot 10^5$	$2.4 \cdot 10^7$
	Re_c	–	$0.6 \cdot 10^5$	$0.6 \cdot 10^5$	$0.6 \cdot 10^5$	$0.2 \cdot 10^7$

[Nm] and angular frequency Ω [min^{-1}] are recorded in the turbine generator. All devices are calibrated to get physical units.

Amongst others, the data are used to determine the ratio α between the velocity in the wake and the inflow of the flume, which is defined by

$$\alpha = u_w/u_1, \tag{1}$$

in which u_1 [m s^{-1}] is the inflow velocity of the flume and u_w [m s^{-1}] is the flow velocity in the wake. The latter is obtained by interpolating the velocity field at three rotor diameters downstream of the rotor swept plane, using the measured vertical and horizontal transects for each test. The ratio α quantifies the amount of kinetic energy extracted from the flow (the so-called velocity deficit) and, together with the wake area, provides the mass flux in the wake. This ratio is therefore a principal indicator of turbine performance in confined channels [5]. In Sec. 4 this parameter will be used as an input to the theoretical model of [3] in order to compare this model to the experimental data.

2.3. Scaling analysis

Although it is not the intent of the experiments to reproduce exactly the flow at the test site, the Eastern Scheldt turbine will nevertheless be referred to as the prototype. In this section, the corresponding model scaling and particular choices made for the test set-up will be explained.

The most important physical processes that should be reproduced in the experimental tests are the flow separation downstream of a hydraulic structure, and the turbine wake and bypass. Their interaction largely determines the power output of a turbine mounted in a hydraulic structure. Therefore, both the flow in the hydraulic structure and at the turbine should be scaled correctly.

2.3.1. Hydraulic structure

A weir is chosen to represent the hydraulic structure, which suffices to represent the flow separation and reattachment of the mean flow [7]. The weir was scaled assuming Froude similitude with the sill-beam of the prototype, for which the flow is subcritical and surface undulations are negligible. Besides, the experimental flow is turbulent, with Reynolds numbers in excess of $\mathcal{O}(10^5)$, such that the results are representative for a full-scale situation [16].

The Froude-number Fr is defined as the ratio between inertia and gravitational forces, and the Reynolds-number Re gives the ratio between inertia and viscous forces in the prototype and model. They are defined, respectively, as

$$Fr = u_1/\sqrt{g h_w}, \tag{2}$$

$$Re = u_1 h_w \rho/\mu, \tag{3}$$

in which u_1 [m s^{-1}] is the inflow velocity of the flume, g [m s^{-2}] is the gravitational acceleration, h_w [m] is the water depth, ρ [kg m^{-3}] the water density, and μ [kg $m^{-1}s^{-1}$] the dynamic viscosity of water. The undisturbed flow velocity, u_1, at full scale is typically 2 m s^{-1}, and the water depth away from the weir amounts to 12 m. The resulting Froude and Reynolds numbers of the flow in the model and prototype are presented in Table 1, demonstrating Froude-similitude and turbulent flow conditions in the flume ($Re > 10^5$) - in accordance with the flow in prototype.

At full scale, the water depth at the weir equals 9 m giving a weir height of 3 m (see Fig. 1c). To assess the influence of the relative weir height on the flow field and power output, weir heights of 0.05 m and 0.10 m were chosen, with corresponding flume depths of 0.65 m and 0.70 m, respectively. Both weirs have a 1:5 upstream slope and a 0.80 m long horizontal crest.

2.3.2. Turbine

The second aspect of the analysis – the flow physics of the horizontal-axis turbine – also involves scaling arguments. To this end, the scaling parameters representing the power output and wake, e.g. chord Reynolds number, the turbine tip-speed ratio and the performance coefficients, should be respected when transforming the flow from prototype scale to the experimental scale [16].

First, the chord Reynolds number needs to be considered, indicating the character (turbulence) of the flow over the blade chord. It is defined as

$$Re_c = u_1 c \rho/\mu, \tag{4}$$

in which c [m] the width of the blade chord. The values in Table 1 are calculated for a blade chord of 0.85 m for the prototype and 0.09 m for the experimental turbine, showing that the experimental flow conditions around the blades are well in the turbulent regime, as is the corresponding flow in prototype. Perfect agreement between Reynolds numbers of model and prototype is not needed to reproduce the hydraulics and often impossible at experimental scale [17].

Second, in order to achieve a realistic reproduction of the turbine wake, the so-called tip speed ratio must be considered. The tip speed ratio, λ, is the tangential velocity of the rotor tip divided by the inflow velocity, defined by

$$\lambda = \left(\frac{2\pi\,\Omega}{60}\,\frac{D}{2}\right) \Big/ u_1, \tag{5}$$

where Ω is the angular frequency [min^{-1}] of the rotor, and u_1 [m s^{-1}] is the inflow velocity. The latter is defined as the depth-averaged velocity at the centre of the inflow section of the flume, where the weir and turbine do not affect the flow. The bed boundary layer is fully developed at this location such that the velocity profile is logarithmic, which is taken into account when determining u_1 from the measurements. Using these definitions, the model turbine is controlled at $\lambda = 4$ which is the same value as in the prototype.

Third, to scale the power production of the turbine properly, the power coefficient and the thrust coefficient of the turbine must be considered. The power coefficient C_P is the turbine power output P [W] relative to the energy flux P_0 [W] of the inflow over the rotor swept area (A_D) which is defined as

$$C_P = P \,/\, P_0 = \left(\mathrm{Q}\,\frac{2\pi\,\Omega}{60}\right) \Big/ \left(\frac{1}{2}\rho u_1^3 A_D\right), \tag{6}$$

in which Q is the torque [N m] exerted on the rotor. Furthermore, the thrust coefficient C_T relates the horizontal force exerted on the turbine T [N] to the momentum flux of the inflow T_0 [N] over the rotor swept area, as follows,

$$C_T = \mathrm{T} \,/\, \mathrm{T}_0 = \mathrm{T} \,/\, \left(\frac{1}{2}\rho u_1^2 A_D\right). \tag{7}$$

The power and thrust coefficients of the model turbine have been determined by SVA Schiffbau Versuchs Anstalt (Potsdam, Germany) in a cavitation tunnel using a Reynolds number, which was five times higher than the Reynolds number used in our tests, for a range of tip speed ratios (see Fig. 3). These power coefficients have been corrected to account for the blockage of the flume walls using the formulation of [5] for a comparison with our tests. The agreement of the curves is excellent indicating both tests operate in

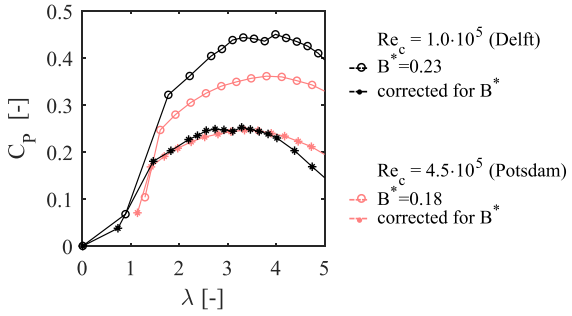

Fig. 3. The measured power coefficient of the experimental turbine at different tip speed ratios in two experimental flumes with different geometry and inflow speed. The power coefficients of the different flumes agree after correction for the flume blockage using [5].

the turbulence regime sufficiently far from the drag crisis around $Re = 2{\cdot}10^3$ [17]. Scaling of the hydraulics in hence acceptable to represent the full-scale conditions [17].

The blockage corrected power curves of Fig. 3 peak at 0.25, which is at the relative low-end of the spectrum for horizontal axis turbines. The strong blade design, with a large blade solidity as inspired by marine propellors, is designed especially for high-blockage conditions and this comes at cost of efficiency when installing them in an unbounded flow.

2.3.3. The combined geometry

Three parameters are used to describe and scale the combined geometry of the flume, weir, and turbine: the relative blockage of the turbine, the relative weir area and the relative streamwise distance of the turbine to the weir.

The swept area of the turbine relative to the channel cross section, the blockage B^* [−], is defined as

$$B^* = A_D / (h_w W), \tag{8}$$

where h_w [m] and W [m] are the depth and width of the flume, respectively. Accordingly, the relative weir height a^* [−] is defined as

$$a^* = h_a / h_w, \tag{9}$$

where h_a [m] is the crest height of the weir. The streamwise distance of the turbine to the weir is scaled with the rotor diameter, using the dimensionless distance x^* [−], defined as

$$x^* = x/D, \tag{10}$$

where D [m] is the rotor diameter. The location $x^* = 0$ is at 10.6 m away from the inflow section of the flume, and corresponds to the trailing edge of the weir (for tests where a weir was present, see Fig. 1b).

The dimensionless blockage and weir height are varied around the prototype values of $B^* = 0.25$ and $a^* = 0.1$, in order to evaluate the effect of these parameters on the power output. In each test series the turbine is mounted at half the water depth locally above the crest of the weir. In a similar fashion the dimensionless rotor distance x^*, which in prototype ranges between −1 during ebb and 1 during flood, is varied between −2 and +2 (see also Table 1). Concluding, the dimensionless scaling parameters of both components of the experimental set-up, the weir and turbine, as well as their combination, are equal to those of the prototype. This implies that the processes reproduced in the experiments are representative for field conditions.

3. Results of the experiments

The generally observed flow pattern is as follows. The flow accelerates towards the weir crest and subsequently expands and slows down over a distance of approximately 7 weir heights downstream. The turbine creates a wake typically extending up to 10 rotor diameters downstream, where the streamwise flow velocities are lower and the turbulence intensities are higher than in the corresponding ambient flow. Overall, the data confirm that the wake configuration is affected by the relative weir area, the blockage, and the turbine position relative to the weir.

Next, we discuss the performance of the turbine in the different test configurations, after which the details of the corresponding flow fields and their influence on the power output are analysed.

3.1. Observed turbine performance

First, as a reference case, the turbine is positioned in a flat-bed flume without a weir. The turbine is operated at a range of tip speed ratios, λ, while its power and thrust are measured. The corresponding power and thrust coefficients are given by the black lines in Fig. 4a and b, respectively. The power curve has a parabolic shape with a maximum around $\lambda \approx 4$. Power output is smaller for higher λ, which is a result of extra drag, as well as for lower λ, which is due to extra stall [18]. These observations confirm the general characteristics of a horizontal-axis turbine.

3.1.1. Varying the rotor distance

Next, for the same water depth and a weir height of 5 cm, the turbine is placed at successive distances x^* from the weir (series 1 of Table 1). Fig. 4 shows that, with a constant tip speed ratio, the power and thrust coefficients generally increase up to 40% with increasing x^*. These coefficients are also larger than for the corresponding reference values (flat bed) for $x^* \geq -1$. The extreme values for the power and thrust coefficient occurred at the limits of the considered range of distances, that is, the observed coefficients are smallest for $x^* = -2$ and largest for $x^* = 2$. Moreover, the optimal tip speed ratio increases from $\lambda \approx 3.5$ for $x^* = -2$ to $\lambda \approx 5$ for $x^* = 2$, with a corresponding increase of the power coefficient C_P from 0.45 to 0.70 (indicated by the black line in Fig. 4).

These effects are partly explained by the additional blockage of the weir, giving an effective, local blockage at the turbine equal to $B^*/(1 - a^*)$, which is larger than the flume blockage B^* [19]. Proposed corrections of the tip speed ratio and the power coefficient to account for the corresponding increase of the flow velocity, in the bypass as well as in the wake. This is confirmed by our measurements for $-1 \leq x^* \leq 1$ if the deformation of the free surface at the weir − another effect influencing blockage − is also taken into account. For $x^* = -2$ and $x^* = 2$ the situation is more complex. Since these turbine locations involve flow contraction and flow expansion, respectively, the associated streamwise gradients of the background flow velocity and pressure fields likely play a role here too in the turbine performance.

3.1.2. Varying the blockage and weir height

In order to investigate the simultaneous effects of blockage and weir height in more detail, the turbine performance is also determined for a larger weir height of 10 cm, giving $a^* = 0.15$ and $a^* = 0.14$, in combination with blockages B^* of 0.25 (series 2) and 0.23 (series 3), respectively. We consider cases where the turbine was operated at $\lambda = 4$ to only study the effect of local blockage and not of tip speed ratio. The corresponding depth-averaged inflow velocities, u_1, velocity coefficients, α, and the power and thrust coefficients, C_T and C_P, are plotted in Fig. 5 as functions of the effective, local blockage $B^*/(1 - a^*)$, as suggested by the results in

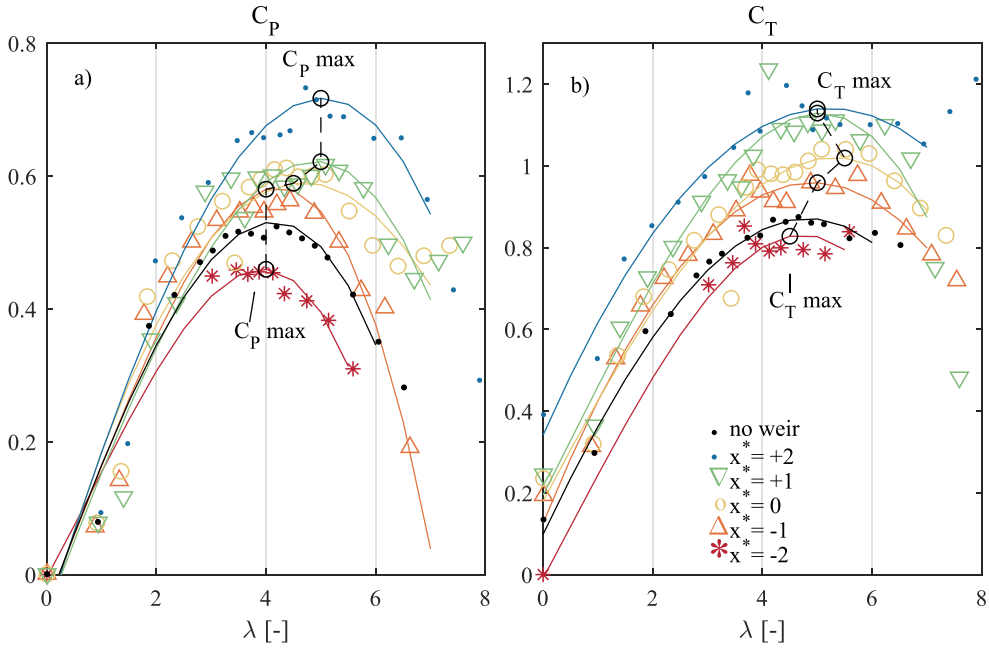

Fig. 4. The measured power coefficient, C_P a) and thrust coefficient, C_T b) of test series 1, $B^* = 0.25$ and $a^* = 0.08$, presented for different tip speed ratios, λ, and for five relative distances of the turbine to the weir end ($-2 \leq x^* \leq 2$). Drawn lines are for illustrative purposes only. They are calculated using a root-mean-square interpolation of the data with a third degree polynomial, a typical shape of a performance curve [18].

Section 3.1.1. Only the data of which effective blockage was varied is displayed to isolate its effect.

The reference velocity u_1 is smaller for series 3 than it is for series 1 and 2, which is a direct consequence of the larger water depth in series 3 to obtain the smaller blockage while the discharge remained unaffected. This difference does not compromise our analysis, since dimensionless quantities are used to characterize turbine performance (i.e., α, C_P and C_T). The relative velocity at the rotor plane, α, is highest for the cases with the largest effective blockage and the highest weir (series 2), moreover if the turbine is situated upstream of the weir. The velocity coefficient is generally smallest if the turbine is positioned at the weir end. Importantly, these results are already corrected to account for the increased local velocity, in other words, they concern effects additional to those caused by the effective blockage only.

As with the variable turbine distance, a larger C_P is generally observed if the effective local blockage is large. The tests with the largest blockage (series 1 and 2) show an increase of the power and thrust coefficients with the turbine distance x^* too, although the effect is comparatively weak for the higher weir (series 2). This trend is not observed for the smaller blockage (series 3). The smallest coefficients occur for the low weir of series 1 and - on average - the highest values for the series with highest effective blockage (series 2). Variation within each series may be explained from the non-uniformity of the flow field at the weir (contraction and expansion), which is examined in the next section.

3.2. Observed flow fields

In the experiments, particular attention is payed to the wake behind the rotor plane as it influences the flow bypassing the turbine and the associated pressure recovery. The latter are principal indicators of turbine performance in confined channels [5]. The wake is here defined as the region downstream of the rotor where the flow velocity amounts to less than ninety percent of the flume inflow velocity, u_1. Important characteristics in this respect are: the horizontal extent and vertical expansion of the wake, and its (a) symmetry. To this end, Fig. 6 shows the observed velocity magnitude, turbulence kinetic energy, and lateral velocity of the flow in a cross section along the centre line of the flume for turbine positions $x^* = -2$ and $x^* = 1$, for constant $\lambda = 4$. The complete data set for all the series of Table 1 and the reference cases are given in the Appendix (Fig. 8).

The presence of a weir generally increases the horizontal extent of the turbine wake. The longest wake is observed for $a^* = 0.15$ and $x^* = -2$, in which case it is five rotor diameters longer than in the case of the turbine without a weir (Fig. 6b). For cases with $a^* = 0.14$ and $a^* = 0.15$, the wake generally extends three to five rotor diameters further downstream than for the cases with $a^* = 0.08$ (see Fig. 6b,c,e, and f).

The vertical expansion of the wake, on the other hand, is reduced if a weir is present, moreover if the turbine is situated upstream of the weir (Fig. 8). Furthermore, the weir enhances the flow beneath the turbine where velocities are approximately 0.5 m s^{-1} larger than in the flow above the turbine. Especially for the smaller blockage (series 2), this asymmetry of the bypass flow is related to the confinement of the wake by the free surface.

In some configurations the horizontal extent and the vertical expansion of the wake influence each other. Recovery of the wake involves a larger downstream distance if the flow is vertically more confined, or if the wake interferes with the flow bypassing the turbine. It is possible that the wake cannot fully expand in these cases due to the flow contraction by the weir (for $x^* = -2$), the high bypass velocity, or the nearby free surface (for $x^* = 1$). The turbulence kinetic energy is particularly high in these situations (centre panels of Fig. 6a,b and d), which suggests a strongly sheared wake flow.

The observed lateral velocity, which is a measure for wake rotation along the streamwise axis, is shown in the right panels of Fig. 6. The rotation in the wake is largest for situations without a weir or when the turbine is situated downstream of the low weir. The confinement of the flow by the weir reduces the wake rotation, possibly due to the increased shear at the interface of the wake and the bypass area. This is substantiated by the observation of a small torque load, which gives the wake its swirling motion.

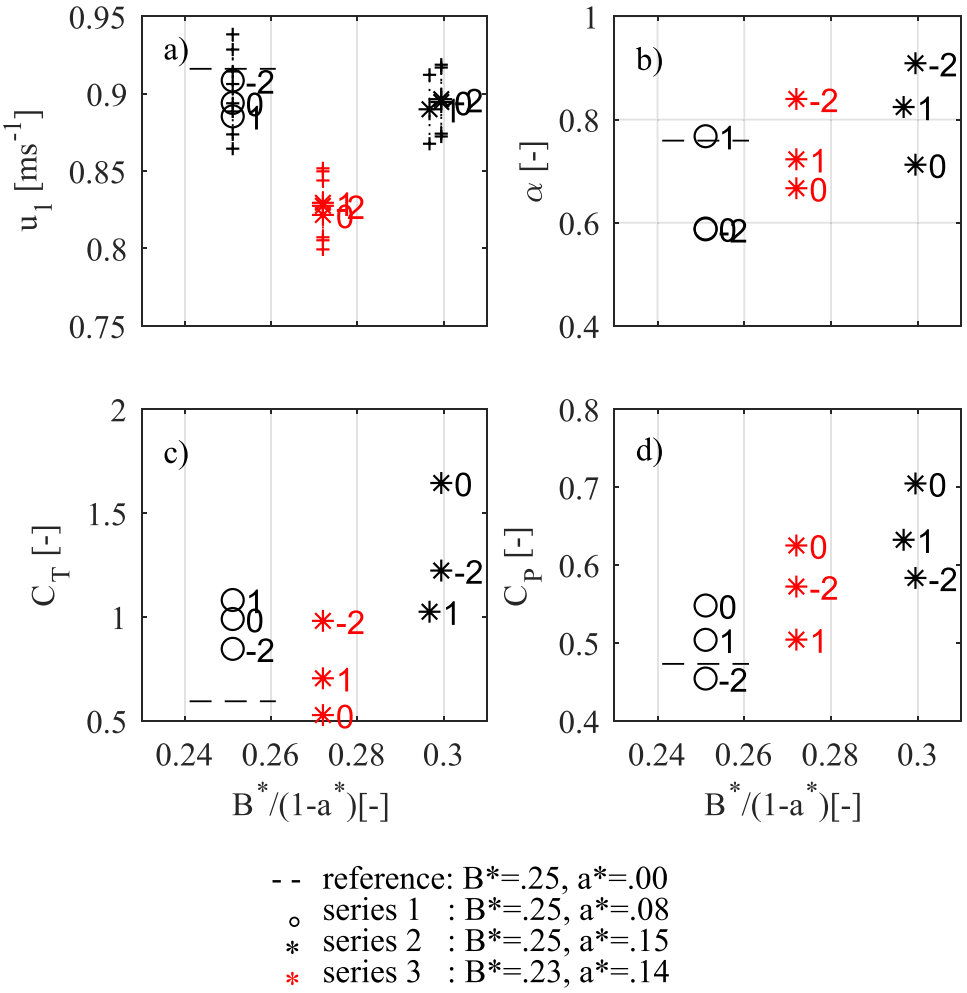

Fig. 5. Time-averaged velocity and performance parameters presented as a function of the effective blockage, $B^*/(1-a^*)$, between the turbine and the weir end. The distance x^* is displayed to the right of each data point. The panels display a) the depth-averaged velocity at the upstream end of the flume and corresponding standard deviation is indicated with an errorbar (symbol "+"), b) the local velocity coefficient in the wake, c) the thrust coefficient, and d) the power coefficient at $\lambda = 4$. The figure presents the subset of the data for which effective blockage was varied.

3.3. Interpretation: inflow and wake effects

In Sec. 3.1 we described that local flow characteristics affected the power coefficient. The power coefficient was generally larger when the turbine was placed at the crest of the weir or downstream thereof, as a result of blockage and a high relative flow velocity at the rotor plane. However, it follows that the power coefficient not only depends on these local characteristics, but also on the upstream and downstream flow pattern as induced by a particular weir-turbine geometry. This flow is e.g. featured by a non-uniform inflow velocity profile for a turbine downstream of the weir (Fig. 6d–f) and a relatively long wake for a turbine upstream of the weir (Fig. 6a–c). The implications of the upstream and downstream flow pattern for the turbine performance will be discussed below.

The characteristics of the flow *upstream* of the turbine affect the power coefficient through its distribution and its streamwise gradients. The flow experiences the largest blockage for an incoming flow, which is uniformly distributed over the cross section [20]. Consequently, the alteration of the vertical velocity profile by an upstream weir can slightly reduce the power coefficient of a downstream turbine. This is relevant for the studied cases for which $x^* > 0$ where we observed a higher velocity below than above the turbine (Fig. 6d–f). Furthermore, streamwise gradients in the incoming flow velocity, as a result of contraction or expansion, may affect the power coefficient. The observed acceleration of the inflow for a turbine at the weir crest likely favoured the power coefficient due to the associated negative streamwise pressure gradient which increases the turbine thrust, such as postulated by Ref. [8].

The flow pattern *downstream* of the turbine also influences the power coefficient, where especially wake expansion plays an important role. A wake with a large vertical (or lateral) extent is associated with a large streamwise pressure difference over the turbine. This follows directly from a theoretical analysis of the flow: if the wake cross-section is larger, the flow velocity in the wake is smaller, hence the resulting pressure difference over the turbine is larger. This explains the comparatively large power output of turbines placed at the trailing edge or downstream of a weir, as the backward-facing step of the weir forces an abrupt expansion of the bypass flow behind the turbine. Furthermore, a long horizontal extent of a confined wake involves smaller gradients in the ambient pressure and hence a smaller pressure drop over the turbine, limiting turbine performance. The ambient pressure gradient is here associated with acceleration of the bypass flow, such as e.g. discussed by Ref. [21]. This explains the non-optimal power output when the turbine is situated upstream of the weir.

While not directly relevant for the power coefficient, the bypass flow may also affect the hydraulic resistance of the turbine-weir

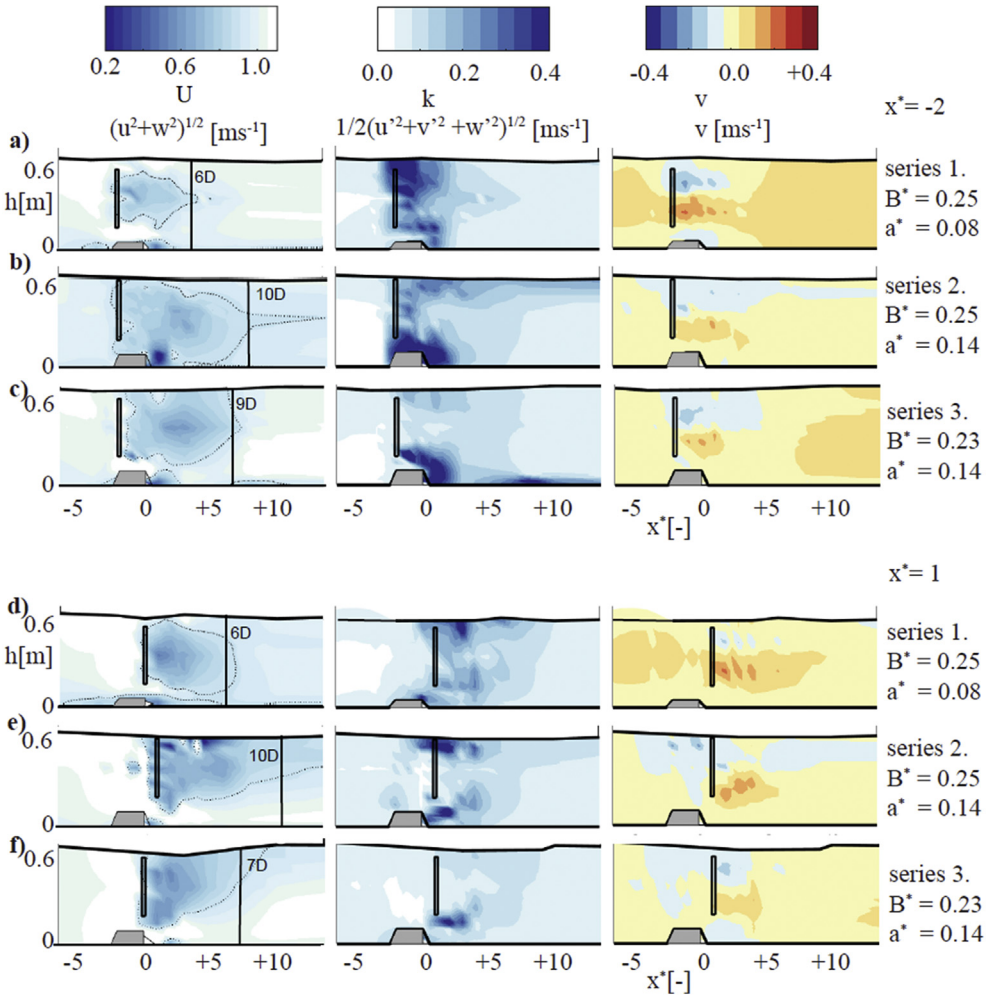

Fig. 6. Measured flow velocity in a streamwise plane at the flume centre line, U, the turbulence kinetic energy, k, in the same plane and the lateral velocity v for all tests. The wake contour (dotted line) in the left-most panels corresponds to a streamwise flow velocity of 90% of the inflow and the vertical line with label indicates the mean wake length. The free surface level displayed is interpolated from the water level data.

combination, and hence the energy yield of the turbine if the flow is controlled by the hydraulic head difference across the structure. This is a consequence of the interaction of the bypass flow with the flow separation downstream of the weir. We observed that the main flow attached at shorter distances to the bed when the turbine is located at the weir end or further downstream ($x^* \geq 0$), compared to situations without a turbine or with a turbine upstream of the weir ($x^* < 0$) (Fig. 6). This substantiates the hypothesis of [22] on the interaction between a weir and a turbine, i.e., the high velocity in the bypass area reduces the length of the recirculation zone downstream of the weir if the turbine is placed at $x^* \geq 0$ [22]. Suggested that, as a consequence, a larger portion of the kinetic energy of the inflow can be harvested by turbines for these configurations.

From the analysed cases, it is concluded that the power coefficient not only depends on the local geometrical parameters at the turbine but also on upstream flow properties and downstream wake properties, sometimes even in a counter-intuitive way. For instance, the power coefficient may still be optimised by adapting the weir as a means of controlling the wake for cases where vertical wake expansion is limited. Theoretical models could provide the necessary framework for analysing the relationship between hydrodynamics and power output for simple turbine-weir geometries.

4. Theoretical modelling

A validation of the theoretical model of [3] against the obtained data set reveals the application range of the model, proving whether or not it can be applied to optimize the geometry of turbine-weir configurations comparable to those considered in the experiments.

4.1. Model description

In the theoretical model the flow is described using one-dimensional balances of mass, energy and momentum postulated by Ref. [5]. Using a momentum-extracting (actuator) disk to describe the action of the turbine, all geometrical information is integrated over the channel width and depth. Additionally, the model schematization of [3] includes an instantaneous step of arbitrary height in the bed as a weir, with downstream a separating flow, and a turbine either upstream or downstream of the weir. The latter determines the configuration of the bypass streamtubes. For the turbine streamtube, the velocity factor, α, is prescribed in the current study (referred to as α_5 in Ref. [3]. The water surface is approximated by means of a stress-free rigid lid.

4.2. Validation results

The power output computed by the model is compared to the experimentally obtained values for a range of λ values ($0 < \lambda < 6$). In Fig. 7 and Table 2 the computed power for the first test series ($B^* = 0.25, a^* = 0.08$) is compared to the corresponding experimentally obtained values. To this end, the results of the analytical model with a turbine upstream of the weir are compared to the experimental results for $x^* = -2, -1$, while the model results with the turbine downstream of the weir are compared with the experiments for $x^* = 1, 2$. The value α in the analytical model is taken as an input as it could be easily obtained from the velocity data.

Table 2 shows that the model performance is generally good for optimal values of the tip speed ratio, $\lambda \approx 4$, with the predicted power output deviating less than 10% from the corresponding experimental results. For $-1 < x^* < 1$ the model also performs well for sub-optimal tip speed ratios, $3 < \lambda < 5$, while for $x^* = -2$ and $x^* = 2$ model results are acceptable only if the tip speed ratio is optimal. The latter is attributed to flow contraction and wake expansion, respectively, that influence the performance of the turbine when it is placed at larger distances from the weir (see section 3.3). These secondary effects are not included in the analytical model which compromises its performance for these turbine positions, especially if the tip speed ratio is sub-optimal. Overall, regardless of the value of x^*, the model performance is poor for tip speed ratios $\lambda <$ ca. 3. In these cases the experimental results are influenced by flow separation and the associated energy losses at the blades, a process which is ignored in the theoretical model, leading to smaller power values. Similarly, for λ slightly larger than 4, where increased drag in the experiments leads to a lower relative wake velocity (α), a process which is not part of the theoretical model. We therefore continue our analysis by considering the model accuracy at optimal tip speed ratio, which is also the more relevant case in practice.

Regarding the turbine, the tip speed ratio and blade shape are not specified directly in the model, but represented by an energy-extracting disk lumping all design and operational information into velocity coefficients. This approach assumes uniformity of the flow velocity and turbine properties over the turbine swept area, which generally leads to an overestimation of the power output as compared to the non-uniformity of the actual situation [23]. Similarly, the blockage by the turbine has been assumed uniform in the model, while in the experiments it is larger in the vertical than in the horizontal direction. We may speculate that the flow in the experiment may therefore experiences slightly less blockage, resulting in a lower power output (Draper et al., 2016).

Regarding the wake flow, in particular the streamwise distance between the turbine and weir affects power output since this influences the wake expansion and flow redistribution in the wake and bypass. By varying this distance the observed power output could change by 40%, as shown in Fig. 4. This effect is not explicitly accounted for in the theoretical model, as it is assumed that the turbine wake does not interfere with the recirculation zone behind the weir. This is a reasonable assumption if the turbine-weir distance is relatively small. To increase the application range of the model to larger values of x^*, however, a more precise schematization of the wake based on the actual distance x^* would be necessary. Another model limitation related to wake expansion concerns the schematization of the free surface by means of a rigid lid. While the position of the rigid lid is chosen with care, based on the mean water level measured, undulations of the free surface near the turbine, as observed in the experiments, are absent in the model. This implies that while the first order effect of the free surface, the blockage, is included in the theoretical model, second order influence of undulations is not. The latter refers to the ambiguous influence of the free surface, which may either constrain the expansion of the wake and thereby reduce the power output, such as discussed by Ref. [19]; or increase the blockage and efficiency due to flow contraction at the turbine position as described by Ref. [24]. Depending on which of these processes dominates, the model is too optimistic or too pessimistic a this point, respectively.

Despite all these simplifications, the model results are reasonably accurate for operational values of λ. We therefore conclude that the current model is valid for a well-defined set of practical cases. A first condition is that the horizontal and vertical blockage should be approximately the same, to ensure that local blockage at the turbine is equal to the prescribed geometric blockage in the model. Next, the model should only be used to predict the power output near the maximum of the power curve, which in this case is at $\lambda = 4$. The user of the model should also be aware that the

Table 2
The tip speed ratio λ and wake velocity coefficient α_5 corresponding to the power estimates presented in Fig. 7. The table shows that the model is most accurate (within ten percent) for the test situations with $-2 < x^* < 2$ and $\lambda \approx 4$.

x^* [−]	λ [−]	α_5 [−]	P_{test} [W]	P_{model} [W]	relative error power [%]
−2	–	0.82	3.3	20.2	511
−2	2.3	0.77	7.0	22.3	217
−2	3.0	0.58	23.1	27.1	17
−2	4.1	0.61	22.8	25.7	13
−2	5.1	0.68	20.0	24.0	20
−1	1.3	0.79	6.3	18.5	192
−1	2.2	0.61	19.9	24.0	21
−1	3.1	0.56	23.3	25.4	**9**
−1	4.2	0.61	24.5	24.0	**−2**
−1	5.3	0.67	21.7	22.3	**3**
+1	0.9	0.98	3.4	12.8	270
+1	2.4	0.76	17.4	23.9	38
+1	2.9	0.81	23.2	21.1	**−9**
+1	4.1	0.77	23.7	23.9	**1**
+1	5.1	0.77	24.3	23.9	**−1**
+2	1.0	1.10	3.5	12.8	263
+2	2.5	0.95	20.2	20.5	**2**
+2	2.9	0.91	22.3	21.1	**−6**
+2	4.3	0.90	23.6	21.1	−11
+2	5.2	0.90	25.9	21.1	−18

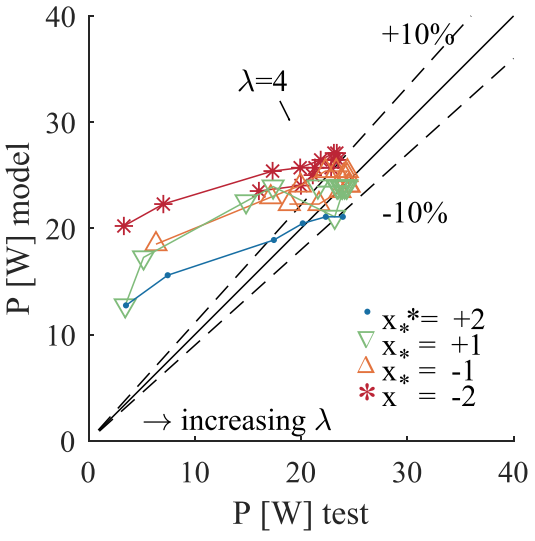

Fig. 7. The power estimations from the model of [3] for a turbine downstream of a weir and upstream of a weir compared to experimental data.

prescribed velocity coefficient in the rotor plane or wake, α, may apply to a specific turbine design. Depending on the application, it can hence be useful to prescribe the velocity factor in the bypass or thrust coefficient (referred to as β_5 and C_T respectively in Ref. [3]) to the theoretical model instead of the α. Lastly, the current model assumes a simple shape of the wake to predict the performance, limiting its use to the turbine-structure distances considered in this work. Three-dimensional computational fluid dynamics must be considered if more accurate performance estimates are required.

5. Discussion

The presented experimental and theoretical analysis applies to hydro-kinetic turbines in a geometry consisting of a channel, which is narrow relative to the turbine diameter, combined with an abrupt step of small height in the bed. This geometry represents the case of a river passing a sluice gate with a weir. We argue that in such situations the local flow condition, governed by the effective blockage and the wake velocity coefficient, is the main factor influencing the turbine performance. The associated geometry range targeted in this study is characterised by a blockage, B^*, between 0.1 and 0.7, a relative step height, a^*, between 0.1 and 0.3, and a distance of the rotor swept plane to the step in the bed of at most two rotor diameters, corresponding to $-2 < x^* < 2$. Beyond this range other processes affect the power coefficient as well, in particular the streamwise and vertical flow velocity gradients, for which the accuracy of the proposed theoretical model is limited.

In large-scale applications of this technology, multi-turbine systems can be installed in multi-gate barriers. Noteworthy is that the power coefficient of a single gate with turbines, as presented in this article, is then affected by the flow through the neighbouring gates as well. For this reason, optimising the lateral distribution of turbines in a barrier is a direction of future research. As a first step [3], already proved the validity of the theoretical model for arrayed deployments of turbines upstream or downstream of a weir, based on detailed information of the flow in the rotor plane and wake from field measurements. For comparable geometries, the predictive capability of the theoretical model can likely be improved to an accuracy of 10% if the flow distribution in the neighbouring wakes and bypasses is schematised explicitly in the theoretical model, such as in the work of [10].

Where this article focused on clarifying influences of the geometry on the power coefficient, the practical implementation of hydro-turbines involves the optimisation of the energy yield and the induced flow resistance as well. With regard to the latter, the optimal turbine configuration in a hydraulic structure may differ from the optimal position presented in this work. This can be explained as follows. The energy yield is the product of both the power coefficient and the ambient flow velocity cubed. If the ambient flow is driven by external water level differences, as for instance caused by the tide, the ambient flow velocity is also influenced by the resistance of the turbine-weir geometry. A high power coefficient will then reduce the ambient flow velocity if the overall resistance experienced by the flow is increased, which is referred to as 'channel-choking' by Ref. [10]. The additional resistance is associated with expansion losses in, respectively, the turbine wake and in the flow separation zone downstream of the weir. Streamlining the flow in these regions could minimize the added resistance, bearing in mind that this will only lead to a larger energy yield if the power coefficient is not significantly reduced. Future research should indicate how such considerations would affect the optimum turbine position and velocity induction regarding energy yield.

Interestingly, the experimental results already point at the existence of a geometry where both the power coefficient and energy yield are high and the added flow resistance is limited. In particular, flow separation and expansion downstream of the weir are suppressed if the turbine is placed at the weir end, while the power coefficient was close to optimal for this position. This offers the opportunity to optimize the design achieving both a high energy yield and a limited additional resistance. The latter is also relevant if the environmental impact of turbine arrays should be minimized. The turbines in the Eastern Scheldt barrier - which were an inspiration for the presented experiments of this work - already benefit from this phenomenon during the tidal flood phase, as discussed in the work of [22].

6. Conclusion

The aim of this study was to clarify the consequences of placing a tidal turbine in a hydraulic structure with regard to the turbine performance. Unique experimental measurements of turbine power and wakes were performed to meet this aim. The influence of weir height, blockage, and streamwise distance between turbine and weir on the power coefficient and associated hydrodynamics was evaluated. Besides, the measurements were used to validate an analytical model for predicting the power output, which is based on a simplified representation of the flow. Combining experiments and theoretical modelling gave insight into the processes that affect the power output of turbines in hydraulic structures, and into the application range of the proposed analytical model.

The power coefficient generally increases if a turbine is placed in a hydraulic structure, which is a result of the increased local blockage. The data reveals a close link between the power coefficient and the observed flow patterns. Upstream, local, as well as downstream flow effects determine the performance. Local effects concern the effective blockage and relative flow velocity in the rotor plane. Effects resulting from the flow upstream and downstream of the rotor concern the velocity distribution in the inflow, bypass and wake, and the streamwise velocity gradients of the background flow. Depending on the position of the turbine relative to the weir, one or a combination of these processes affects its performance.

The power coefficient increased with up to 40% when the turbine was re-positioned from two rotor diameters upstream of the weir to two diameters downstream of the weir. Over this range, in successive order, flow contraction, local effective blockage and flow expansion dominated the physics at the turbine. Most power could be harvested if the local blockage was highest, that is, when the turbine was placed at the structure crest, but only when allowing space for a favourable wake configuration.

The influence of local effects on the power coefficient could be well predicted with the theoretical model, within 10% accuracy, making it a promising tool to maximise power for the different control variables within this range. The model has limitations for geometries beyond the studied range of $x^* = \pm 2$, in which processes of flow contraction and expansion become increasingly important. By including more information, particularly on the wake configuration, the application range of the model could be extended to include these configurations. In this way this work advances the knowledge needed to meet targets on renewable energy.

CRediT authorship contribution statement

M.C. Verbeek: Conceptualization, Investigation, Writing - original draft, Visualization. **R.J. Labeur:** Supervision, Writing - review & editing, Funding acquisition. **W.S.J. Uijttewaal:** Supervision.

Declaration of competing interest

The authors declare that they have no known competing financial interests or personal relationships that could have appeared to influence the work reported in this paper.

Acknowledgements

This work is financed by the Netherlands Organisation for Scientific Research (NWO) within the research programme The New Delta with project number 869.15.008. We are grateful to Tocardo B.V. for the use of the blades and hub of their experimental turbine. The European Regional Development Fund (ERDF) OP-Zuid 2014–2020 programme is acknowledged for their support. A special thanks goes to the personnel of DEMO and Environmental Fluid Mechanics laboratory of TU Delft for their assistance in the tests.

Appendix

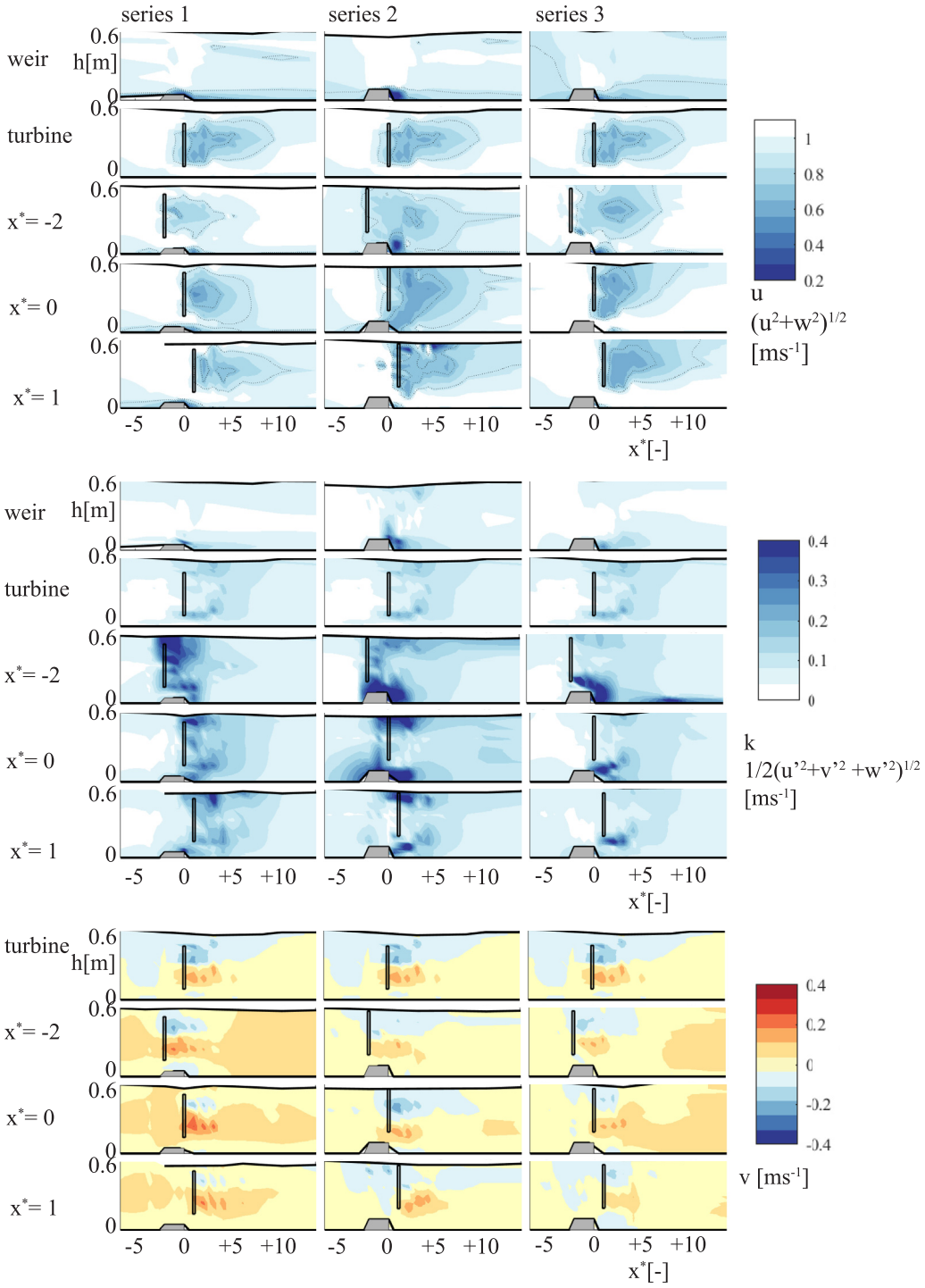

Fig. 8. Measured flow velocity in a streamwise plane at the flume centre line, the turbulence intensity in the same plane and the lateral velocity in this plane for all tests.

References

[1] European Committee, A Policy Framework for Climate and Energy in the Period from 2020 to 2030. Tech. Rep. COM(2014), Jan. 2014, 15, Communication from the commission to the parlement, Brussels, p. 6. URL ec.europa.euclimapoliciesstrategies2030_en.

[2] A.S. Bahaj, Generating electricity from the oceans, Renew. Sustain. Energy Rev. 15 (7) (2011) 3399–3416.

[3] M. Verbeek, R. Labeur, W. Uijttewaal, The performance of a weir-mounted tidal turbine: field observations and theoretical modelling, Renew. Energy 153 (2020) 601–614.

[4] T.S.D. O'Mahoney, A. de Fockert, A. Bijlsma, P. de Haas, Hydrodynamic impact and power production of tidal turbines in a storm surge barrier, in: 13th EWTEC, 2019.

[5] C. Garrett, P. Cummins, The efficiency of a turbine in a tidal channel, J. Fluid Mech. 588 (2007) 243–251.

[6] T. Stallard, R. Collings, T. Feng, J. Whelan, Interactions between tidal turbine wakes: experimental study of a group of three-bladed rotors, Phil. Trans. Math. Phys. Eng. Sci. 371 (2013), 1985.

[7] B. Hofland, Rock and Roll Turbulence-Induced Damage to Granular Bed Protections, Ph.D. thesis, Delft University of Technology, 2005.

[8] A. Wimshurst, R. Willden, Tidal power extraction on a streamwise bed slope, Ocean. Eng. 125 (2016) 70–81.

[9] R. Vennell, Tuning turbines in a tidal channel, J. Fluid Mech. 663 (2010) 253–267.

[10] T. Nishino, R.H.J. Willden, The efficiency of an array of tidal turbines partially blocking a wide channel, J. Fluid Mech. 708 (2012) 596–606.

[11] A. Betz, Das maximum der theoretisch möglichen ausnützung des windes durch windmotoren, Z. Das Gesamte Turbinenwesen Heft 26 (1920). Seiten 307 bis 309.

[12] F. Lanchester, A contribution to the theory of propulsion and the screw propeller, Trans. Inst. Naval Architect. 57 (1915) 98–116.

[13] I. Milne, A. Day, R. Sharma, R. Flay, The characterisation of the hydrodynamic loads on tidal turbines due to turbulence, Renew. Sustain. Energy Rev. 56 (2016) 851–864.

[14] W. Batten, M. Harrison, A. Bahaj, Accuracy of the actuator disc-rans approach for predicting the performance and wake of tidal turbines, Phil. Trans. Math. Phys. Eng. Sci. 371 (2012).

[15] A.S. Nortek, Operations manual – Vectrino. Nortek group, red, Norway, URL, nortekgroup.com/products/vectrino, 2019. (Accessed 17 October 2019).

[16] A. Bahaj, L. Myers, Shaping array design of marine current energy converters through scaled experimental analysis, Energy 59 (2013) 83–94.

[17] L. Myers, A. Bahaj, An experimental investigation simulating flow effects in first generation marine current energy converter arrays, Renew. Energy 37 (1) (2012) 28–36.

[18] T. Burton, D. Sharpe, N. Jenkins, E. Bossanyi, Aerodynamics of Horizontal-Axis Wind Turbines, Wiley-Blackwell, 2002, pp. 41–172. Ch. 3.

[19] A. Bahaj, A. Molland, J. Chaplin, W. Batten, Power and thrust measurements of marine current turbines under various hydrodynamic flow conditions in a cavitation tunnel and a towing tank, Renew. Energy 32 (3) (2007) 407–426.

[20] S. Draper, T. Nishino, T.A.A. Adcock, P.H. Taylor, Performance of an ideal turbine in an inviscid shear flow, J. Fluid Mech. 796 (2016) 86–112.

[21] C. Vogel, G. Houlsby, R. Willden, Effect of free surface deformation on the extractable power of a finite width turbine array, Renew. Energy 88 (2016) 317–324.

[22] M.C. Verbeek, R.J. Labeur, A.C. Bijlsma, T.S.D. O'Mahoney, How bathymetric features affect turbine performance: insights from a cfd model, in: 7th Oxford Tidal Energy Workshop 8-9 April 2019, 2019, pp. 13–14. Oxford, UK.

[23] S. Draper, T. Nishino, Centred and staggered arrangements of tidal turbines, J. Fluid Mech. 739 (2014) 72–93.

[24] J.I. Whelan, J.M.R. Graham, J. Peiro, A free-surface and blockage correction for tidal turbines, J. Fluid Mech. 624 (2009) 281–291.